International Journal of Physics, 2026, Vol. 14, No. 2, 36-47
Available online at http://pubs.sciepub.com/ijp/14/2/3
Published by Science and Education Publishing
DOI:10.12691/ijp-14-2-3

Characterization of UAV-Based Free-Space Optical (FSO) Channel Under Real Atmospheric Conditions in the Tropical Savanna Region of Korhogo, Northern Côte d'Ivoire

Wongnigué Allassane Soro[1,*], Amadou Soumahoro[1], Douatia Koné[1,2], Aladji Kamagaté[1]

[1]Mathematics Physics Chemistry, LaTIATE Laboratory, Université Peleforo Gon Coulibaly, Korhogo, Côte d'Ivoire
[2]Research and Technological Innovation Department, Ecole Supérieure Africaine des Technologies de l'Information et de la Communication, Abidjan, Côte d'Ivoire
*Corresponding author: soro.wongnigue@upgc.edu.ci

Received July 05, 2026; Revised August 07, 2026; Accepted August 14, 2026

Abstract Unmanned aerial vehicle (UAV)-assisted free-space optical (FSO) communication is a promising solution for rapidly deployable, high-capacity wireless networks. However, realistic channel characterization in tropical environments remains challenging because atmospheric attenuation, turbulence, pointing errors, and angle-of-arrival (AoA) fluctuations are often investigated independently and rarely using long-term site-specific meteorological data. This paper presents a unified statistical framework for modeling a UAV-assisted FSO link under the tropical savanna climate of Korhogo, northern Côte d'Ivoire. The proposed model jointly incorporates weather-dependent attenuation caused by rain, fog, humidity, and dust, Málaga-distributed atmospheric turbulence, pointing errors, and AoA fluctuations within a heterodyne-detection decode-and-forward relay architecture. Atmospheric attenuation parameters are derived from six years (2020–2025) of meteorological observations collected by the Korhogo station of the National Meteorological Agency (ANAM), enabling realistic channel characterization. Closed-form channel statistics are employed to evaluate the signal-to-noise ratio (SNR) and bit-error rate (BER). The results show seasonal atmospheric attenuation ranging from 0.81 dB/km during the dry season to 3.10 dB/km under severe rainy conditions. Increasing the UAV altitude from 200 m to 500 m extends the communication range from 2.5 km to 4.5 km for an SNR threshold of 10 dB, while the reliable transmission distance at a BER of 10^{-3} increases from 2.5 km to 3.2 km. More importantly, the analysis reveals a distance-dependent altitude trade-off. Beyond approximately 5 km, humidity-induced attenuation and beam divergence outweigh turbulence mitigation, challenging the common assumption that higher UAV altitudes always improve FSO performance. These findings provide practical design guidelines for deploying reliable UAV-assisted FSO systems in tropical environments.

Keywords: *Angle-of-Arrival fluctuations, Atmospheric attenuation, Atmospheric turbulence, Channel characterization, Málaga distribution, Pointing errors, UAV-FSO communications*

Cite This Article: Wongnigué Allassane Soro, Amadou Soumahoro, Douatia Koné, and Aladji Kamagaté, "Characterization of UAV-Based Free-Space Optical (FSO) Channel Under Real Atmospheric Conditions in the Tropical Savanna Region of Korhogo, Northern Côte d'Ivoire." *International Journal of Physics*, vol. 14, no. 2 (2026): 36-47. doi: 10.12691/ijp-14-2-3.

1. Introduction

The rapid evolution of modern communication networks, driven by bandwidth-intensive applications such as the Internet of Things (IoT), autonomous systems, and cloud services, has significantly increased the demand for high-capacity, low-latency, and reliable wireless connectivity. Conventional radio-frequency (RF) systems are increasingly constrained by spectrum congestion, limited bandwidth, and electromagnetic interference [1]. Free-Space Optical (FSO) communication has emerged as a promising complementary technology, offering large bandwidth, high data rates, immunity to electromagnetic interference, and cost-effective deployment without requiring extensive infrastructure [2,3]. Unmanned Aerial Vehicles (UAVs) further enhance these capabilities by providing flexible line-of-sight connectivity and rapid deployment, making them attractive as aerial relays for surveillance, disaster response, emergency communications, and broadband connectivity in hard-to-reach areas [4]. Nevertheless, the performance of UAV-assisted FSO links remains highly sensitive to atmospheric conditions and platform dynamics. Atmospheric attenuation caused by rain, fog, humidity, and dust, atmospheric turbulence, pointing errors resulting from transmitter-receiver misalignment, and angle-of-arrival (AoA) fluctuations induced by UAV motion can significantly degrade communication reliability [3,5].

Accurate statistical channel modeling is therefore essential for realistic performance evaluation and system design. The Lognormal distribution is commonly adopted for weak turbulence, whereas the Gamma-Gamma and K distributions are widely used under moderate-to-strong turbulence conditions [6,7]. However, these models remain restricted to specific turbulence regimes. The Málaga distribution overcomes this limitation by providing a unified statistical framework capable of accurately representing weak, moderate, and strong atmospheric turbulence within a single analytical model [8]. Owing to its flexibility and excellent agreement with Monte Carlo simulations, it has become one of the most suitable channel models for UAV-assisted FSO communications [9].

In West Africa, few studies have investigated FSO link performance under site-specific meteorological observations, and none have addressed UAV-specific impairments. Ajewole *et al*. characterized fog- and rain-induced attenuation for a terrestrial link in Akure, Nigeria, using one year of visibility and rain-rate data, but their analysis was confined to a fixed ground-to-ground geometry [10]. Kone *et al*. [9] demonstrated the dominant influence of rain and fog attenuation in a coastal urban environment, though without considering the atmospheric conditions of tropical savanna regions such as Korhogo. More recently, Lawal et al. characterized fog-induced attenuation across four Nigerian climatic zones, including the Sahel savanna city of Kano, using fifteen years of visibility data, capturing Harmattan-driven seasonal variability relevant to savanna environments [11]. Across these studies, atmospheric characterization has so far been limited to fixed terrestrial links, leaving platform dynamics, atmospheric turbulence, pointing errors, and AoA fluctuations, all central to UAV-assisted FSO performance, unaddressed. Despite these advances, three important research gaps remain. First, existing studies mainly focus on coastal, temperate, or fixed terrestrial deployments, while the specific atmospheric conditions of tropical savanna regions under UAV-based mobility, characterized by Harmattan dust events, pronounced seasonal humidity variations, and strong thermal gradients, remain largely unexplored. Second, atmospheric attenuation, turbulence, pointing errors, and AoA fluctuations are often analyzed independently rather than within a unified statistical framework, although their combined effects determine the actual channel performance. Third, only a few studies rely on long-term site-specific meteorological records to jointly characterize all major impairments affecting UAV-assisted FSO channels.

To address these gaps, this paper presents an integrated characterization of a UAV-assisted FSO link under the site-specific atmospheric conditions of Korhogo, a tropical savanna region in northern Côte d'Ivoire. Beyond its scientific contribution, this work is motivated by the growing need for reliable broadband connectivity in rural areas and by emerging applications such as precision agriculture, where UAV-assisted FSO communications offer an attractive alternative for high-capacity wireless backhaul. To the best of our knowledge, this is the first study combining long-term meteorological records archived by the Korhogo station of the National Meteorological Agency (ANAM) with a unified Málaga-based channel model incorporating atmospheric attenuation, turbulence, pointing errors, and AoA fluctuations. The main contributions of this paper are summarized as follows:

- Development of a unified statistical channel model jointly accounting for atmospheric attenuation due to rain, fog, humidity, and dust, Málaga-distributed atmospheric turbulence, pointing errors, and angle-of-arrival (AoA) fluctuations, representative of one hop of a UAV-based decode-and-forward relay system.
- Statistical characterization based on meteorological records archived by the Korhogo station of the National Meteorological Agency (ANAM) over the period 2020–2025, capturing the climatic variability of a tropical savanna environment and providing realistic channel parameters for UAV-assisted FSO communications.
- SNR and BER evaluation that UAV altitude and propagation distance jointly govern link reliability and revealing, to the best of our knowledge, a previously unreported distance-dependent reversal of the altitude benefit under site-specific atmospheric conditions.

2. Study Area and System Model

2.1. Study Area

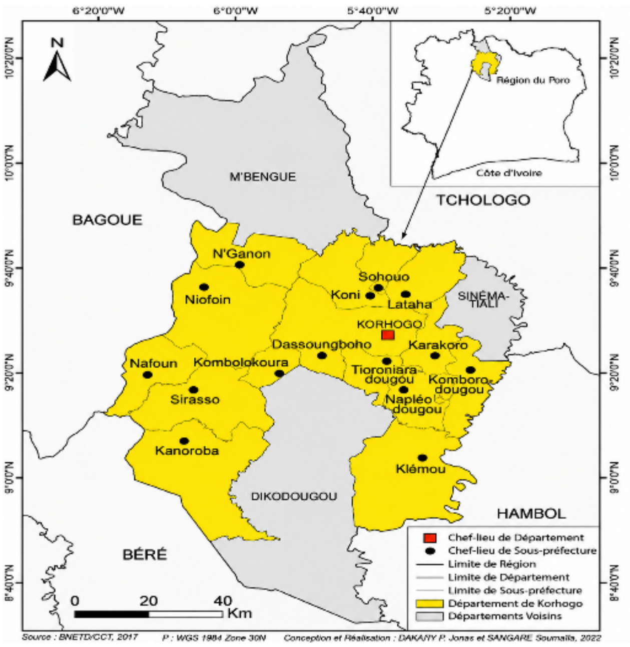

Figure 1. Geographic location of Korhogo, the capital city of the Poro Region [14]

The study area considered in this work is the city of Korhogo, located in northern Côte d'Ivoire, in the savanna region, where it serves as the administrative capital of the Poro Region (Figure 1). The climate of Korhogo is classified as tropical savanna according to the Köppen climate classification [12]. It is characterized by two distinct seasons: a dry season extending from November to March, marked by high temperatures, low precipitation, and low relative humidity, and a rainy season from April to October, characterized by higher rainfall levels with two precipitation peaks generally observed in June and September [13].

These climatic variations create highly dynamic environmental conditions that directly affect FSO communication links. Accurate modeling of these dynamic is essential for evaluating and optimizing the performance of UAV-FSO links to ensure reliable communication under local climatic constraints.

2.2. System Model

Beyond its scientific interest, the UAV-assisted FSO link studied here offers a promising means of extending next-generation (5G/6G) broadband connectivity to rural areas. It also has prospective applications in precision agriculture, such as crop monitoring, particularly relevant to tropical environments like northern Côte d'Ivoire. The system consists of a free-space optical link between a ground station and a UAV acting as an aerial relay, as shown in Figure 2. This link represents either hop of a decode-and-forward (DF) relay deployment, the ground-to-UAV (G2U) uplink or the UAV-to-ground (U2G) downlink. The UAV receives, decodes, and forwards the optical signal between two ground stations. Heterodyne detection (HD) is adopted at the receiver for its high sensitivity and its robustness against atmospheric turbulence [8].

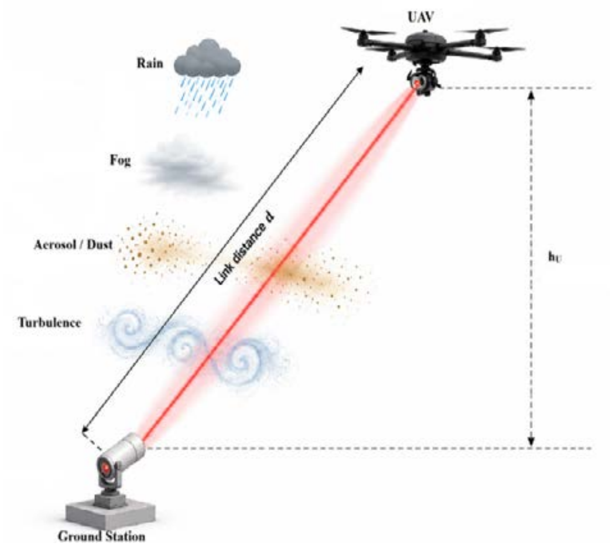

Figure 2. Architecture of the proposed UAV-FSO system

The FSO channel is modeled by accounting for the main physical phenomena affecting optical wave propagation through the atmosphere. It is represented by a positive real coefficient *h*, which quantifies the overall degradation experienced by the optical signal during propagation. The channel coefficient follows a multiplicative model that separates the contributions of the different impairment mechanisms:

$$h = h_{at} h_{tur} h_{pe} h_{AoA}. \quad (1)$$

Here, h_{at} denotes atmospheric attenuation caused by absorption and scattering, h_{tur} represents turbulence-induced fading, h_{pe} accounts for the loss due to pointing errors between transmitter and receiver and h_{AoA} captures link degradation or interruption resulting from angle-of-arrival (AoA) fluctuations and residual UAV motion.

This model accounts for both the principal atmospheric impairments (rain, fog, humidity, and dust) and geometric perturbations affecting UAV-FSO links under the atmospheric conditions of Korhogo.

2.2.1. Atmospheric Attenuation

Atmospheric attenuation is a major factor affecting the performance of Free-Space Optical (FSO) systems. It results from the absorption and scattering of the optical beam by atmospheric constituents such as fog droplets, rain, water vapor, and dust particles. In this study, atmospheric attenuation is modeled as a deterministic loss that depends on weather conditions and propagation distance. For the optical link, the attenuation coefficient follows the Beer-Lambert law [10,17]:

$$h_{at,k} = \exp\left(-\frac{\alpha_{at} d_k}{4.343}\right), \quad (2)$$

where d_k (km) is the propagation distance and α_{at} (dB/km) is the total atmospheric attenuation coefficient, expressed as:

$$\alpha_{at} = \alpha_{fog} + \alpha_{rain} + \alpha_{hum} + \alpha_{dust}. \quad (3)$$

Where α_{fog}, α_{rain}, α_{hum}, and α_{dust} denote the attenuation coefficients due to fog, rain, humidity, and dust, respectively.

Fog attenuation is modeled using the Kim model, which relates optical attenuation to meteorological visibility [23,24]:

$$\alpha_{fog} = \frac{3.91}{V}\left(\frac{\lambda}{550}\right)^{-q}. \quad (4)$$

With:

$$q = \begin{cases} 1.6; if \;\; V > 50 \\ 1.3; if \; 6 < V < 50 \\ 0.16V + 0.34; if \; 1 < V < 6 \\ V - 0.5; if \; 0.5 < V < 1 \\ 0; if \;\; V < 0.5 \end{cases} \quad (5)$$

Where V (in km) denotes the visibility distance, λ (in nm) refers to the operating wavelength, 550 is a reference wavelength.

Rain attenuation results from the absorption and scattering of light by raindrops. Although generally less severe than fog attenuation, it can significantly affect FSO links in tropical regions during the rainy season. The specific attenuation associated with the rainfall rate R (mm/h) is modeled as [9,19]:

$$\alpha_{rain} = aR^b. \tag{6}$$

In this equation, α_{rain} represents the specific attenuation due to rain, α is a constant, R is the rainfall rate, and b is an attenuation coefficient. For the rainfall conditions observed in Korhogo $(R < 3.8mm/h)$, $a = 0.509$ and $b = 0.63$ are adopted [9].

Humidity attenuation is associated with the absorption of optical energy by atmospheric water vapor contained within the propagation path. The corresponding attenuation coefficient (α_{hum}), depends on the precipitable water content χ and is expressed in dB/km as [20].

$$\alpha_{hum} = \begin{cases} \dfrac{10}{\ln 10}\exp\left(-A_i\chi^{0.5}\right); si\ \chi < \chi_i \\ 10\left[B_i \log_{10}\left(\dfrac{\chi_i}{\chi}\right)\right] - \log_{10} k_i; si\ \chi \geq \chi_i \end{cases}. \tag{7}$$

The precipitable water χ content is defined as the vertical integral of specific humidity along the atmospheric column and can be approximated as a function of the UAV altitude (h_U) under the assumption of small variations in air (ρ_{air}) density and specific humidity (q_v).

$$\chi = \frac{\rho_{air} q_v}{\rho_w} h_U. \tag{8}$$

Where ρ_w denotes the water density. The specific humidity q_v is determined from atmospheric temperature T (°C), pressure P (hPa), and relative humidity R_H (%) according to:

$$q_v = \frac{0.622e}{P - 0.378e}. \tag{9}$$

Where e the partial water vapor pressure is given by:

$$e = \frac{R_H}{100} e_s(T) \text{ with } e_s(T) = 6.112\exp\left(\frac{17.67T}{T + 243.5}\right).$$

For an operating wavelength of 1550 nm, the empirical parameters of the adopted model are $A_i = 0.211$, $B_i = 0.111$, $k_i = 0.802$, and $\chi_i = 1.1$, as reported for FSO communication systems [20].

Dust particles suspended in the atmosphere scatter and absorb the laser beam. This reduces the received optical power and increases the bit error rate. Dust storms may also reduce visibility, disrupt transportation. The dust-induced attenuation is modeled using an extinction coefficient derived from Mie scattering and absorption theory. It depends on particle concentration, and is expressed in (dB/km) as follows [21]:

$$\alpha_{dust} = 4.434 \times 10^3 N_d \sigma_{ext}. \tag{10}$$

Where N_d is the volumetric concentration of dust particles, expressed in terms of particulate matter (PM) concentration as $N_d = \frac{3C_{PM}}{4\pi\rho_d r_d^3}$. And the term σ_{ext} is the extinction cross-section from Mie theory, $\sigma_{ext} = \pi Q_{ext} r_d^2$. Here, C_{PM} is the mass concentration of suspended particles (kg/m^3), $\rho_d = 2500\,kg/m^3$ is the density of Sahelian dust particles, r_d is the average particle radius (m). This study considers PM2.5 and PM10 particles.

2.2.2. Atmospheric Turbulence Modeling Using the Málaga Distribution

In addition to meteorological attenuation, atmospheric turbulence significantly affects optical signal propagation in UAV-FSO systems. It arises from random fluctuations in the air refractive index caused by variations in temperature, pressure, and humidity. These fluctuations induce scintillation, beam spreading, and phase distortions, which degrade the quality of the received signal [3]. The turbulence strength is characterized by the refractive-index structure parameter C_n^2 ($\mathrm{m}^{-2/3}$). For low-altitude UAV-FSO links, its vertical profile is modeled using the Hufnagel-Valley model [22].

$$C_n^2(h_U) = 2.7 \times 10^{-16} e^{-h_U/1500} + Ae^{-h_U/100}. \tag{11}$$

Where $A = C_n^2(0)$ characterizes near-ground turbulence. In this study, $C_n^2(0) = 8.4 \times 10^{-14}\ \mathrm{m}^{-2/3}$, corresponding to the nighttime refractive-index structure parameter [9].

The turbulence-induced scintillation strength is quantified by the Rytov variance:

$$\sigma_{R,k}^2 = 1.23 C_n^2(h_U)\left(\frac{2\pi}{\lambda}\right)^{7/6} \mathrm{d}^{11/6} \tag{12}$$

The Málaga distribution is adopted to statistically characterize turbulence-induced fading, as it provides a unified framework encompassing several classical models, including the Lognormal, Gamma–Gamma, and K distributions [23]. The probability density function (PDF) of the normalized irradiance I is expressed as [24]:

$$f_I(I) = \frac{1}{I}\frac{\alpha^{\alpha/2}}{\Gamma(\alpha) g^{1+\alpha/2}}\left(\frac{g\beta}{g\beta + \Omega'}\right)^{\beta+\alpha/2} \sum_{m=1}^{\beta} b_m$$

$$\times G_{1,2}^{2,0}\left(\frac{\alpha\beta}{g\beta + \Omega'} I \middle|\, \begin{matrix} 1 \\ m, \alpha \end{matrix}\right). I \geq 0 \tag{13}$$

Where $\Gamma(.)$ denotes the Gamma function, $G_{p,q}^{m,n}(\cdot)$ represents the Meijer-G function.

The parameters g and Ω' are related to the composition of the received optical field. The term $g = 2b(1-\tau)$ represents the average power of the off-axis scattered component, where $2b$ is the total average power of the scattered components and τ is the fraction of power coupled to the line-of-sight (LOS) component. The parameter $\Omega' = \Omega + 2b\tau + 2\sqrt{2b\tau\Omega}\cos(\theta_A - \theta_B)$ denotes the effective average power of the coherent (LOS) component, including both direct and coupled contributions. It depends on Ω, $2b\tau$, and the phase interference between the scattered and LOS components, characterized by the phases θ_A and θ_B.

The coefficient $b_{m,k}$ is a combinatorial weighting factor defined as: $b_m = \binom{\beta-1}{m-1}\frac{1}{(m-1)!}\left(\frac{\Omega'}{g\beta}\right)^{m-1}, m \in \{1,2,\ldots,\beta\}$

The parameter α describes fluctuations associated with large turbulent eddies, whereas $\beta \in \mathbb{N}^+$ represents the number of scattering cells related to small-scale turbulence. These parameters are determined from the Rytov variance σ_R^2 as follows :

$$\alpha = \left[\exp\left(\frac{0.49\sigma_R^2}{\left(1+1.11\sigma_R^{12/5}\right)^{7/6}}\right)\right]^{-1},$$

$$\beta = \left[\exp\left(\frac{0.51\sigma_R^2}{\left(1+0.69\sigma_R^{12/5}\right)^{5/6}}\right)\right]^{-1}.$$

2.2.3. Degradation Due to Pointing Errors

In UAV-FSO systems, pointing errors are a major source of channel degradation. UAV vibrations, platform instability, and atmospheric disturbances cause random misalignment between the optical beam and the receiver aperture. Assuming a Gaussian beam profile and a circular receiver aperture, the pointing loss is expressed as [5,25,26]:

$$h_{pe} = A_0 \exp\left(-\frac{2r_d^2}{w_{eq}^2}\right). \quad (14)$$

Where $A_0 = [erf(\upsilon)]^2$ denotes the collected power fraction under perfect alignment, and $r_d = \sqrt{x_d^2 + y_d^2}$; with $x_d, y_d \sim \mathcal{N}(0, \sigma_d^2)$, is the radial displacement of the beam centroid on the receiver plane. The pointing displacement is modeled as a Rayleigh random variable resulting from independent Gaussian horizontal and vertical offsets with variance σ_d^2. The total pointing variance combines both UAV jitter and atmospheric beam wander effects :

$$\sigma_d^2 = d^2\sigma_\theta^2 + K_{bw}C_n^2(h_U)d^3\omega_0^{-1/3}. \quad (15)$$

Where σ_θ^2 denotes the UAV angular jitter variance. The coefficient K_{bw} groups the model constants and depends on the turbulence regime. In this work, the value $K_{bw} = 1.44$ is adopted [18].

The equivalent beam radius ω_{eq}, which accounts for the finite size of the receiver aperture, is given by:

$$\omega_{eq} = \omega^2 \frac{\sqrt{\pi}\,\mathrm{erf}(\upsilon)}{2\upsilon\exp(-\upsilon^2)}. \quad (16)$$

With $\omega = \omega_0\sqrt{1+\left(\frac{d}{z_R}\right)^2\left(1+\frac{2\omega_0^2}{\rho^2}\right)}$ and $\upsilon = \frac{r\sqrt{\pi}}{\omega\sqrt{2}}$, where r is the radius of the receiver lens, ω_0 the beam waist radius, $z_R = \frac{\pi\omega_0^2}{\lambda}$ the Rayleigh range and $\rho = \left[0.55C_n^2(h_U)\left(\frac{2\pi}{\lambda}\right)^2 d\right]^{-3/5}$ the atmospheric coherence radius (Fried parameter).

The probability density function (PDF) of the pointing error loss is :

$$f_{h_{pe}}(h) = \frac{\zeta^2}{A_0^2} h_k^{\zeta^2-1}. \qquad 0 \le h \le A_{0,k} \quad (17)$$

With $\zeta = \frac{\omega_{eq}}{2\sigma_d}$ is the pointing error severity parameter.

2.2.4. Degradation Due to Angle-of-Arrival (AoA) Fluctuations

In practical UAV-FSO links, atmospheric turbulence not only affects the beam intensity but also induces random angular deviations at the receiver plane. These fluctuations are referred to as angle-of-arrival (AoA) errors. They can significantly impact link reliability, especially under narrow field-of-view (FOV) constraints. The AoA error θ_a is modeled as a Rayleigh-distributed random variable [5]:

$$f_{\theta_a}(\theta_a) \approx \frac{\theta_a}{\sigma_a^2}\exp\left(-\frac{\theta_a^2}{2\sigma_a^2}\right).\theta_a \ge 0 \quad (18)$$

Here, σ_a^2 is the AoA variance, which quantifies the angular fluctuations caused by atmospheric turbulence. Assuming a constant refractive-index structure parameter along the propagation path, the AoA variance is given by:

$$\sigma_a^2 = 2.91(2r)^{-1/3}C_n^2(h_U)d. \quad (19)$$

Due to the limited receiver field of view θ_FOV, AoA fluctuations induce a binary loss mechanism: the link is preserved $(h_{AoA} = 1)$ when $\theta_a \le \theta_{FOV}$, and lost $(h_{AoA} = 0)$ otherwise. Hence, h_{AoA} is a Bernoulli-type random variable with probability mass function:

$$f_{h_{AoA}}(h) = p_0\delta(h) + (1 - p_0)\delta(h-1). \quad (20)$$

Where:

$$p_0 = 1 - \int_0^{\theta_{FOV}} \frac{\theta_a}{\sigma_a^2}\exp\left(-\frac{\theta_a^2}{2\sigma_a^2}\right)d\theta_a = \exp\left(-\frac{\theta_{FoV}^2}{2\sigma_a^2}\right).$$

2.2.5. Overall Channel Degradation

The optical propagation between the ground stations and the UAV is affected by several physical impairments, including atmospheric attenuation, atmospheric turbulence, pointing errors, and angle-of-arrival (AoA) fluctuations. Assuming that these effects are statistically independent, the PDF of the overall FSO channel gain given in Equation 1 for link k can be expressed as [3]:

$$f_h(I) = \int_0^{\infty} \frac{1}{Z} f_{h_{AoA}}\left(\frac{I}{Z}\right) f_z(Z)\,dZ. \quad (21)$$

With Z being the conditional random variable defined as: $Z = h_{at} I h_{pe}$. Since h_{at} is a positive deterministic parameter, the PDF of Z can be derived from the Málaga turbulence model combined with the pointing error statistics. Substituting this expression into (21), the PDF of the overall channel gain h is obtained as:

$$f_h(I) = p_0\delta(I) + (1-p_0)B\sum_{m=1}^{\beta} b_m \times (AI)^{\zeta^2-1} G_{2,3}^{2,1}\left(\frac{A}{A_0}I \middle| \begin{matrix} 1,\zeta^2 \\ m,\alpha,\zeta^2-1 \end{matrix}\right). \quad (22)$$

With :

$$B_k = \frac{\zeta^2}{A_0^2}\frac{\alpha^{\alpha/2}}{\Gamma(\alpha)g^{1+\alpha/2}}\left(\frac{g\beta}{g\beta+\Omega'}\right)^{\beta+\alpha/2}\frac{1}{h_{at}^{\zeta^2}}$$

$$A = \frac{\alpha\beta}{(g\beta+\Omega')h_{at}}.$$

2.3. SNR and BER Analysis

2.3.1. Instantaneous SNR

Assuming heterodyne detection (HD) at the optical receiver, the received signal is affected by the channel gain, additive Gaussian noise, and the opto-electronic conversion efficiency of the photodetector. It is expressed as [27,28]:

$$y = R\sqrt{P_{LO}P_r}\,x + n. \quad (23)$$

Where x denotes the transmitted optical signal, R is the photodetector responsivity, P_{LO} is the local oscillator power, $P_r = P_t h$ is the received optical power, and $n \sim N(0,\sigma_n^2)$ represents additive white Gaussian noise (AWGN).

The instantaneous signal-to-noise ratio (SNR) is therefore given by:

$$\gamma = \frac{R^2 P_{LO} P_t}{\sigma_n^2} h \cong \overline{\gamma} h. \quad (24)$$

Where $\overline{\gamma_k}$ is the average electrical SNR. Under a background-radiation-limited regime, the noise variance is expressed as:

$$\sigma_n^2 = 4\pi q R N_b B_e B_0 A_r \left(1 - \cos(\theta_{FoV})\right). \quad (25)$$

Where q is the electron charge, B_e is the electrical bandwidth, N_b is the background optical radiance, B_0 is the optical filter bandwidth, $A_r = \pi r^2$ is the receiver aperture area, and $\theta_{FoV,k}$ is the receiver field-of-view half-angle.

Using the relationship $\gamma = \overline{\gamma \mathrm{h}}$, the PDF of the instantaneous SNR is obtained as:

$$f_\gamma(\gamma) = p_0\delta(\gamma) + (1-p_0)B\sum_{m=1}^{\beta} b_m \frac{A^{\zeta^2-1}}{\overline{\gamma}^{\zeta^2}} \times \gamma^{\zeta^2-1} G_{2,3}^{2,1}\left(\frac{A}{A_0\overline{\gamma}}\gamma \middle| \begin{matrix} 1,\zeta^2 \\ m,\alpha,\zeta^2-1 \end{matrix}\right). \quad (26)$$

2.3.2. Bit Error Rate (BER)

The bit error rate (BER) is a key performance metric for assessing the reliability of optical communication systems. In this work, coherent binary phase-shift keying (BPSK) is adopted for its robustness against noise and its compatibility with heterodyne detection (HD) and decode-and-forward (DF) relaying. The average BER is defined using the Gaussian Q-function as $BER = \mathbb{E}\left[Q\left(\sqrt{2\gamma}\right)\right]$, which, using the unified BER representation with $p = 1/2$ and $q = 1$ for coherent BPSK, can be written as [23].

$$BER = \frac{q^p}{2\Gamma(p)}\int_0^{\infty} \exp(-q\gamma)\gamma^{p-1} f_\gamma(\gamma)\,d\gamma. \quad (27)$$

Substituting the SNR PDF from Equation (22) and applying standard Meijer-G integral identities yields the following closed-form expression:

$$BER = \frac{1}{2}p_0 + \frac{(1-p_0)}{2\sqrt{\pi}}B\sum_{m=1}^{\beta} b_m \frac{A^{\zeta^2-1}}{\overline{\gamma}^{\zeta^2}} \times G_{3,3}^{2,2}\left(\frac{A}{A_0\overline{\gamma}} \middle| \begin{matrix} 1,\zeta^2,3/2-\zeta^2 \\ m,\alpha,\zeta^2-1 \end{matrix}\right). \quad (28)$$

3. Results and Discussions

3.1. Results

This section presents numerical results based on the mathematical framework developed earlier. These results highlight the combined effects of atmospheric turbulence and geometric impairments on UAV-FSO link performance. The atmospheric analysis relies on daily meteorological records archived by the Korhogo station of the National Meteorological Agency (ANAM) over the period 2020-2025 [29]. The dataset comprises daily measurements of total precipitation, maximum relative humidity, average visibility, maximum air temperature, and maximum atmospheric pressure. On the basis of this period, typical aerosol concentration values were taken from the work of Gnamien *et al*. [30], who reported PM2.5 and PM10 measurements for Korhogo. The remaining simulation parameters are listed in Table 1.

Table 1. Simulation parameters used for the UAV-FSO system [23,26,27,31]

Parameter	Value
Wavelength, λ	1550 nm
Receiver aperture radius, $\boldsymbol{r}$	0.1 m
Transmitter beam radius, $\boldsymbol{\omega_0}$	0.02 m
Photodetector responsivity, $\boldsymbol{R}$	0.9 A/W
Optical bandwidth, $\boldsymbol{B_0}$	10 nm
Electrical bandwidth, $\boldsymbol{B_e}$	1 GHz
Background radiance, $\boldsymbol{N_b}$	10^{-3}W/m²/sr/Hz
Mie extinction factor, $\boldsymbol{Q_{ext}}$	2
PM2.5 / PM10 concentration[5]	218 /534µg/m³
Phase difference, $\boldsymbol{\theta_A - \theta_B}$	π/2 rad
Málaga parameter, b	0.1079
Málaga parameter, τ	0.596
Málaga parameter, Ω	1.3265

3.1.1. Evaluation of Atmospheric Attenuation

Figure 3 presents the temporal variation of the total atmospheric attenuation coefficient over the period 2020-2025. The results show pronounced seasonal and interannual fluctuations, with values ranging from 0.81 dB/km to 3.10 dB/km and an average of 1.29 dB/km. The highest attenuation was recorded in September 2023, coinciding with a period of intense atmospheric moisture, consistent with the peak rainfall period generally observed between June and September in Korhogo. Consistent with the tropical savanna climate of Korhogo, atmospheric attenuation is systematically higher during the rainy season and lower during the dry season. During the wet season, abundant atmospheric water vapor, frequent rainfall, and high relative humidity enhance optical absorption and scattering along the propagation path. In contrast, the dry season is characterized by lower humidity and improved visibility, although occasional Harmattan dust may locally affect atmospheric transparency. Consequently, the overall attenuation remains significantly lower than during the rainy season. Atmospheric attenuation therefore depends heavily on the seasonal weather conditions in the Korhogo region.

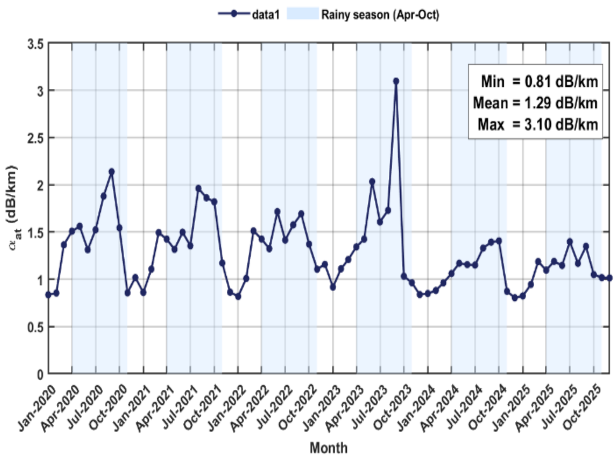

Figure 3. Monthly variation of the total atmospheric attenuation coefficient at an altitude of 500 m over the period 2020 - 2025

3.1.2. Impact Analysis of Atmospheric Turbulence

Using the turbulence parameter $A = C_n^2(0) = 8.4\times10^{-14}\ \mathrm{m}^{-2/3}$, which is used throughout the simulations, Figure 4 presents the evolution of the scintillation index σ_R^2 with propagation distance for different UAV altitudes. The results show a marked increase in σ_R^2 with distance and a marked decrease with altitude, at 10 km σ_R^2 drops from approximately 16 at 200 m to nearly 1 at 500 m, a reduction of more than 90%. This behavior is consistent with Rytov theory. A longer horizontal propagation distance increases the accumulation of turbulence effects, leading to a higher scintillation index. Conversely, a higher UAV altitude is associated with lower C_n^2 values, which reduce turbulence-induced scintillation. This near-ground decay of C_n^2 is particularly pronounced in the study area, where intense solar heating of the bare savanna soil during the dry season generates strong temperature gradients between the ground and the lowest atmospheric layers, sustaining vigorous near-surface convective turbulence that fades rapidly above a few hundred meters.

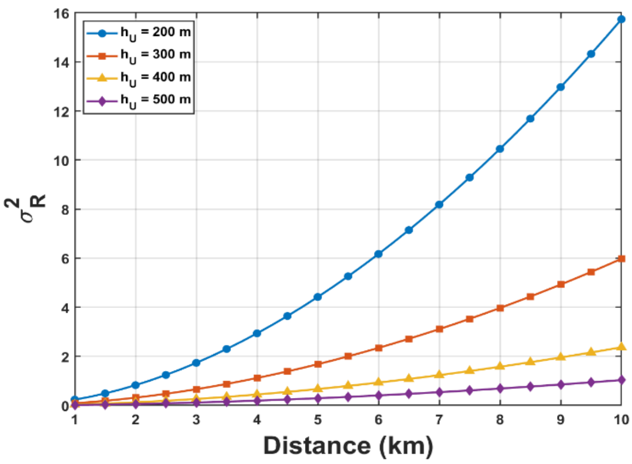

Figure 4. Evolution of scintillation as a function of link distance for different altitudes

3.1.3. Pointing Error Analysis

Figure 5 presents the evolution of the pointing error severity parameter ζ with propagation distance for different UAV altitudes, for a fixed RMS angular jitter of 50 μrad. The parameter ζ decreases rapidly as distance increases, then saturates toward values below unity, reflecting the progressive degradation of alignment between the transmitted beam and the receiver aperture as the beam radial displacement grows. The critical threshold $\zeta = 1$, marking the transition from a weak pointing-error regime to a strongly degradation-limited regime, is reached between approximately 3 km and 4.5 km depending on UAV altitude. This behavior is closely related to the stronger optical turbulence prevailing in the lower atmospheric layers, where larger refractive-index fluctuations increase beam wander. In the Korhogo environment, these fluctuations become more significant over longer propagation paths, resulting in a progressive deterioration of beam alignment. As the UAV altitude increases, the optical beam traverses layers characterized by lower values of the refractive-index structure parameter C_n^2, thereby reducing beam wander and delaying the onset of severe pointing errors.

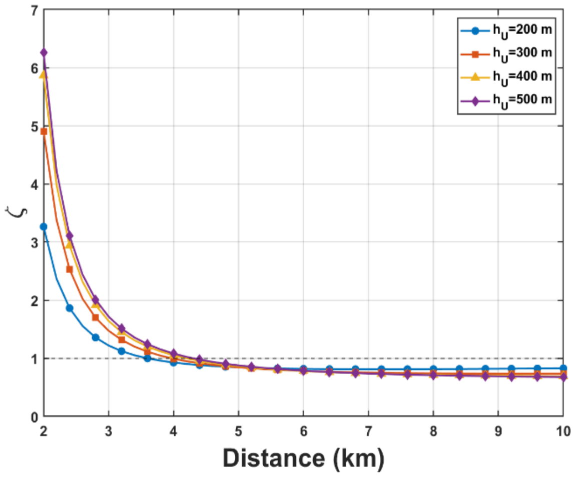

Figure 5. Variation of the pointing error severity parameter ζ with link distance for different UAV altitudes $(\sigma_\theta = 50\mu rad)$

3.1.4. Analysis of Angle-of-Arrival (AoA) Fluctuations

Angle-of-arrival (AoA) fluctuations are a direct consequence of atmospheric turbulence in optical wireless links. As the optical beam propagates, random refractive-index fluctuations continuously perturb its propagation direction, producing angular deviations at the receiver. Figure 6 illustrates the evolution of the AoA standard deviation σ_a with propagation distance for UAV altitudes ranging from 200 m to 500 m.

The AoA standard deviation increases monotonically with propagation distance at all altitudes because successive angular deviations accumulate along the optical path. At 200 m, σ_a reaches approximately 25 μrad at 10 km, whereas it remains close to 6 μrad at 500 m over the same distance. Intermediate UAV altitudes produce intermediate values. As discussed in Section 3.1.2, this improvement results from the progressive reduction of atmospheric turbulence with altitude. In our study area, the lower atmospheric layers exhibit stronger refractive-index fluctuations, making the optical beam more susceptible to angular deviations over long propagation paths.

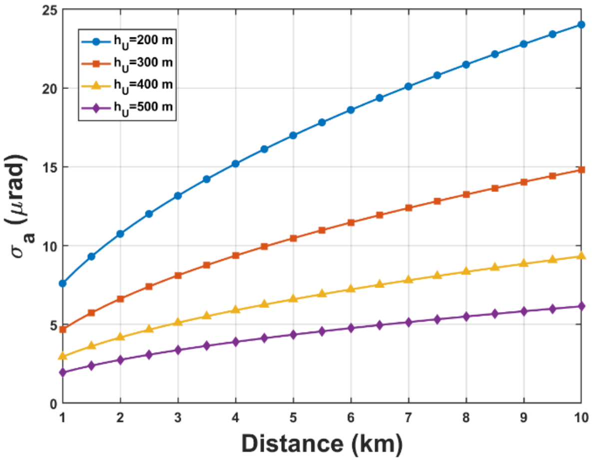

Figure 6. Variation of the angle-of-arrival standard deviation with link distance

3.1.5. SNR and BER Performance Analysis

Having characterized the individual contributions of atmospheric attenuation, turbulence, pointing errors, and AoA fluctuations, this section evaluates their combined effect on system-level performance through the SNR and BER metrics, in order to assess overall link reliability under real atmospheric conditions in Korhogo.

3.1.5.1. SNR Performance Analysis

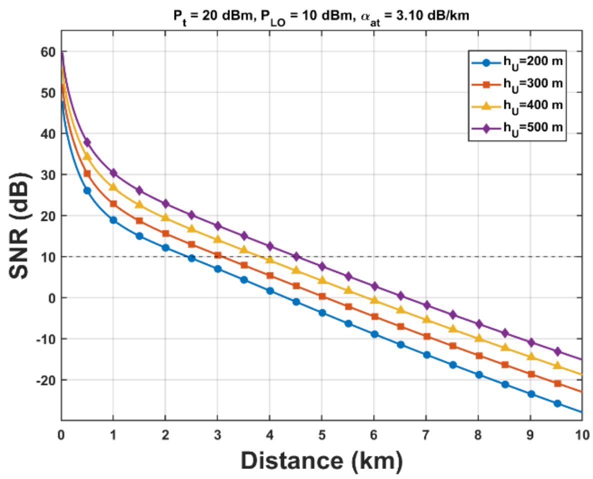

Figure 7. SNR versus link distance for different UAV altitudes

The SNR decreases continuously with propagation distance at all altitudes. At short distances (< 1 km), it remains high, between 20 and 40 dB, indicating good link quality. As distance increases, propagation losses combined with atmospheric attenuation, turbulence, pointing errors, and AoA fluctuations progressively degrade the received power; the curves eventually turn negative beyond approximately 4.5 to 7 km, depending on altitude. Considering a minimum operating threshold of SNR = 10 dB, the maximum transmission distances are approximately 2.5, 3, 4, and 4.5 km for UAV altitudes of 200, 300, 400, and 500 m, respectively. This improvement with altitude is consistent with the previous results. As the

UAV operates at higher altitudes, the optical beam propagates through more stable atmospheric layers, reducing turbulence-induced impairments and improving the received signal quality. The resulting increase in channel stability improves the received SNR and extends the achievable transmission distance.

3.1.5.1. BER Performance Analysis

Figure 8 illustrates the average BER versus propagation distance for UAV altitudes of 200, 300, 400, and 500 m under the worst atmospheric attenuation condition ($\alpha_{at} = 3.10$ dB/km). Up to approximately 5 km, increasing the UAV altitude significantly improves link reliability. For example, at 3 km, the BER decreases from 6×10^{-3} at 200 m to 3×10^{-3} at 500 m, owing to the weaker atmospheric turbulence and the resulting reduction in pointing errors and angle-of-arrival (AoA) fluctuations. Taking $BER = 10^{-3}$ as the reliability criterion, the maximum achievable communication range extends from approximately 2.5 km at 200 m to 3.2 km at 500 m, highlighting the benefit of operating at higher altitudes over short-to-medium propagation distances. Beyond approximately 5 km, the BER curves intersect and the performance trend reverses. At longer distances, the increased atmospheric attenuation associated with higher UAV altitudes, driven by the altitude-dependent humidity coefficient (Eq.7-8), together with the larger beam divergence induced by the longer propagation path, progressively outweighs the turbulence mitigation achieved at higher elevations. Consequently, these cumulative propagation losses become dominant, leading to slightly lower BER values at lower altitudes over extended transmission distances.

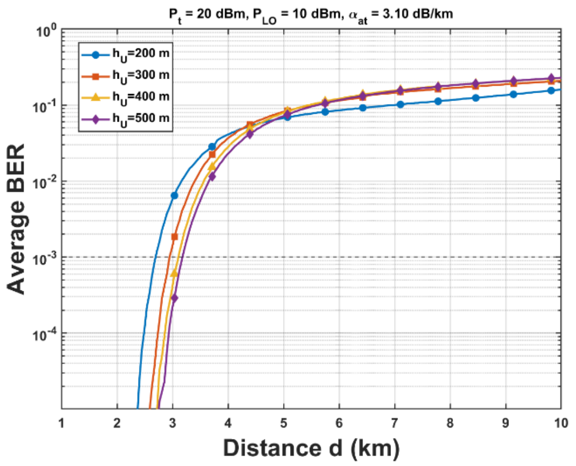

Figure 8. Average BER versus propagation distance for different UAV altitudes

As shown in Figure 9, the average BER decreases monotonically with increasing SNR for all UAV altitudes, dropping from approximately 10^{-1} at low SNR to nearly 10^{-6} at high SNR. The performance remains strongly dependent on the UAV altitude. At 200 m, the BER reaches an error floor of approximately 5×10^{-6} beyond 30 dB, whereas at 500 m, the 10^{-6} threshold is achieved at only 16 dB. This improvement results from the weaker turbulence conditions encountered at higher altitudes, which reduce channel impairments as discussed in the previous sections. Beyond approximately 15 dB, the BER curves progressively flatten, indicating that further SNR improvements yield only marginal performance gains. In this high-SNR regime, thermal noise becomes negligible, and the residual errors are mainly dominated by turbulence-induced channel fluctuations and misalignment effects. The BER curves progressively approach the AWGN reference, indicating that atmospheric impairments become less pronounced under more favorable propagation conditions. Consequently, increasing the UAV altitude reduces the SNR required to achieve a given BER target, thereby enhancing the overall reliability of the FSO link.

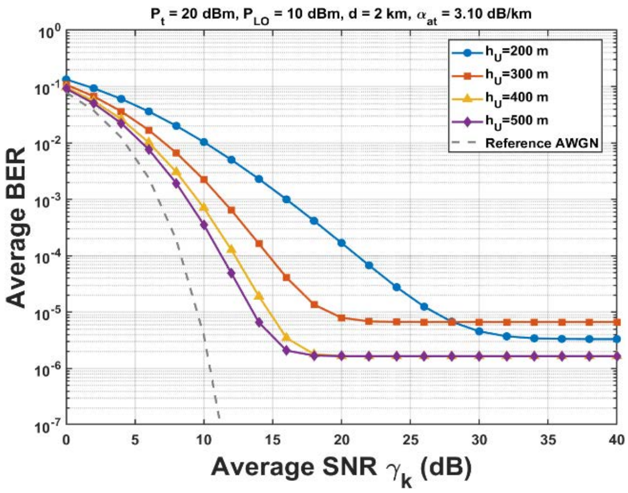

Figure 9. BER performance evaluation of a UAV-FSO link at 2 km with $\alpha_{at} = 3.10$ dB/km, $FoV = 5\sigma_a$, $P_t = 20$ dBm and $P_{LO} = 10$ dBm

To assess the impact of atmospheric attenuation on link reliability, the average BER is evaluated as a function of SNR for a fixed UAV altitude of $h_U = 200m$ and a propagation distance of $d = 2km$ (Figure 10). Four propagation scenarios are considered: an attenuation-free channel and three atmospheric attenuation levels $\alpha_{at} = 0.81;1.29$, and 3.10 dB/km, corresponding to the minimum, mean, and maximum values obtained (Figure 3). Higher atmospheric attenuation systematically shifts the BER curves toward higher SNR values. Under the most severe attenuation (3.10 dB/km), approximately 8–10 dB of additional SNR is required to achieve the same BER as in the attenuation-free case. This behavior results from the reduction in the received optical power caused by absorption and scattering along the propagation path.

Beyond 40 dB, all curves converge to the same error floor of approximately. 2×10^{-6} In this high-SNR regime, the effect of atmospheric attenuation becomes negligible compared with turbulence-induced channel fluctuations and geometric impairments, which dominate the residual error probability. Consequently, atmospheric attenuation mainly affects the SNR required to achieve a target BER, whereas the ultimate performance limit is governed by turbulence and beam misalignment.

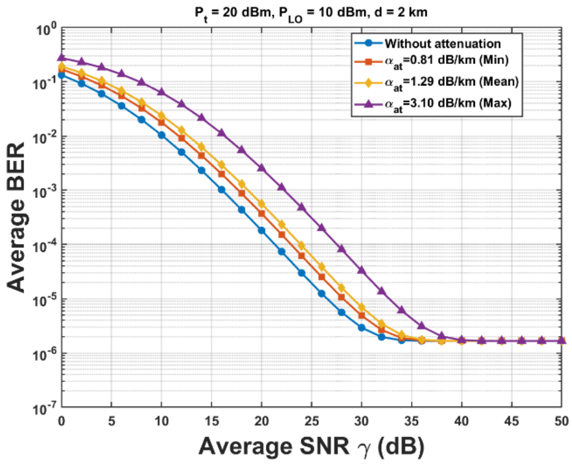

Figure 10. Average BER versus average SNR for different atmospheric attenuation levels (2 km with $FoV = 5\sigma_a$, $P_t = 20$ dBm and $P_{LO} = 10$ dBm)

3.2. Discussion

The simulation results provide a comprehensive assessment of UAV-FSO link performance under the climatic conditions of Korhogo. They highlight the combined influence of atmospheric conditions, propagation distance, and UAV altitude on system reliability. The meteorological data retrieved from the archive of ANAM for the period 2020-2025 confirm that atmospheric phenomena significantly affect the operating range and reliability of optical wireless links in this environment.

Atmospheric attenuation exhibits a clear seasonal variation. The highest value, reaching 3.10 dB/km, occurs during the rainy season because of increased humidity and precipitation. Nevertheless, the attenuation levels measured in Korhogo remain moderate compared with those reported for more severe tropical environments [32]. They are also lower than the sandstorm-induced attenuation observed in arid UAV-FSO deployments [16]. These observations indicate that FSO communication remains a viable solution in Korhogo, particularly during the dry season. They are consistent with the findings of Kone *et al*. [9], who identified the rainy season as the most critical period for FSO links in tropical climates.

Beyond the meteorological characterization, the BER analysis provides further insight into how these atmospheric conditions affect communication performance. The BER-versus-distance results reveal that the impact of UAV altitude depends on the propagation distance. At short and medium distances, turbulence-induced impairments remain the dominant limiting factor. Since the near-ground refractive-index structure parameter decreases rapidly with altitude, the effects of scintillation, pointing errors, and AoA fluctuations are significantly reduced. Consequently, increasing the UAV altitude rapidly improves the BER performance, in agreement with recent turbulence-mitigation studies [12,33,34]. A different behavior appears beyond approximately 5 km. At longer propagation distances, humidity attenuation increases because of the precipitable water content described by Eqs. (7) and (8). At the same time, beam divergence becomes more pronounced as the slant propagation path increases. These effects gradually outweigh the benefit obtained from the reduction of turbulence. As a result, the optimum UAV altitude depends on the transmission distance. Higher altitudes are more suitable for short-range rural backhaul links, whereas lower altitudes become preferable for transmission distances approaching 8-10 km. This observation provides practical guidance for UAV-FSO deployment in the Korhogo region and further refines trajectory optimization strategies proposed for fixed-wing UAV-FSO systems [35].

Finally, the obtained BER characteristics are compared with previous Málaga-based UAV-FSO studies. The BER evolution agrees well with the results reported by Shen *et al.* [23] and Xu *et al.* [8], where the BER decreases rapidly with increasing SNR before approaching an error floor determined by residual channel impairments. In the present work, a similar behavior is observed, with the BER approaching approximately 10^{-6} under high-SNR conditions. However, unlike these previous studies, the present analysis demonstrates that the benefit of increasing the UAV altitude is not constant but depends strongly on the propagation distance. This altitude-dependent performance reversal has not been reported for fixed-geometry UAV-FSO links and represents the main contribution of this work to the existing literature.

This study characterizes a single FSO link, representative of either hop of a UAV-based decode-and-forward relay deployment. The closed-form SNR and BER expressions were derived directly from the statistical channel model and verified through consistency checks across the parameter range considered. The end-to-end performance analysis of a two-hop relay system, including the derivation of the overall outage probability and average BER, will be addressed in a subsequent stage of this work.

4. Conclusion

This study presented a statistical characterization of a UAV-assisted FSO link under the real atmospheric conditions of Korhogo. The proposed model combines the Málaga turbulence distribution with the main physical phenomena affecting free-space optical links, namely atmospheric attenuation due to fog, rain, humidity, and dust, atmospheric turbulence, pointing errors, and angle-of-arrival (AoA) fluctuations.

Meteorological records obtained from the archives of the Korhogo station of the National Meteorological Agency (ANAM) over the period 2020-2025 revealed strong seasonal variability in atmospheric attenuation, ranging from 0.81 dB/km in the dry season to 3.10 dB/km under the most adverse rainy conditions. The individual analysis of these degradation mechanisms showed that UAV altitude and propagation distance the two dominant parameters governing channel quality. The SNR and BER analysis then translated these channel characteristics into system-level performance indicators. In the worst-case scenario, corresponding to an attenuation of 3.10 dB/km, the maximum range for an SNR threshold of 10 dB extends from 2.5 km at 200 m altitude to 4.5 km at 500 m altitude. Considering a reliability criterion of $BER = 10^{-3}$, the achievable communication range extends from 2.5 km to 3.2 km as altitude increases from 200 m to 500 m. This benefit is nonetheless not systematic. Beyond approximately 5 km, the increase in humidity attenuation and beam divergence losses becomes dominant over the reduction in turbulence, reversing the trend. The optimal UAV altitude therefore depends on the propagation distance and cannot be treated as a fixed value. Unlike most previous Málaga-based UAV-FSO studies, which generally assume idealized or generic atmospheric conditions, the present work demonstrates that the optimal UAV altitude is jointly determined by the propagation distance and the local atmospheric environment derived from real meteorological measurements. This result nuances the commonly held assumption that a higher altitude is always preferable, and constitutes, to our knowledge, a novel observation among UAV-FSO studies based on real local atmospheric data.

Beyond its scientific interest, this characterization provides concrete guidance for deploying UAV-FSO links aimed at extending 5G/6G broadband connectivity to rural areas of northern Côte d'Ivoire. It also opens prospective applications in fields such as precision agriculture, particularly for crop monitoring. The results yield practical recommendations on the optimal altitude and distance combinations required to maintain a given reliability level under local atmospheric conditions.

Overall, this work provides a realistic framework for the design and performance evaluation of UAV-assisted FSO links in tropical environments, highlighting the importance of jointly optimizing UAV altitude and propagation distance according to real atmospheric conditions rather than relying on fixed deployment assumptions. Future work will focus on extending this single-link characterization toward a full end-to-end analysis of a two-hop decode-and-forward (DF) relay system.

References

[1] Aboelala, O., Lee, I. E., and Chung, G. C. (2022). "A Survey of Hybrid Free Space Optics (FSO) Communication Networks to Achieve 5G Connectivity for Backhauling," Entropy, vol. 24, no. 11, p. 1573.

[2] Mohsan,S. A. H., Khan,M. A., and Amjad,H. (2023). "Hybrid FSO/RF networks: A review of practical constraints, applications and challenges," *Opt. Switch. Netw.*, vol. 47, p. 100697.

[3] Gupta,A., Dhawan, D., and Gupta, N. (2023). "Review on UAV-based FSO links: recent advances, challenges, and performance metrics," *Opt. Eng.*, vol. 63, no. 04.

[4] Wang,J. Y., Ma,Y., Lu, R. R., Wang,J. B., Lin,M., and Cheng, J. (2021). "Hovering UAV-Based FSO Communications: Channel Modelling, Performance Analysis, and Parameter Optimization," *IEEE J. Sel. Areas Commun.*, vol. 39, no. 10, pp. 2946–2959.

[5] Singh,D., and Swaminathan,R. (2022). "Comprehensive Performance Analysis of Hovering UAV-Based FSO Communication System," *IEEE Photonics J.*, vol. 14, no. 5, pp. 1–13.

[6] Badarneh,O. S., El Bouanani,F., Almehmadi,F. S., and Silva,H. S. (2023). "FSO Communications Over Doubly Inverted Gamma-Gamma Turbulence Channels With Nonzero-Boresight Pointing Errors," *IEEE Wirel. Commun. Lett.*, vol. 12, no. 10, pp. 1761–1765.

[7] Duyen,T. H. (2023). "Performance Analysis of FSO DF Relays with Log-Normal Fading Channel," *J. Opt. Commun.*, vol. 44, no. 3, pp. 395–403.

[8] Xu,G., Yu,X., Wang,J., Song,Z., and Zhang,Q. (2024). "Performance Analysis of Multi-UAV Optical Communication Systems Over Foggy Channel Under Málaga Turbulence and Pointing Error Impairments," *IEEE Photonics J.*, vol. 16, no. 6, pp. 1–16.

[9] Kone,D.,SORO,P. A., and Kamagaté,A. (2024) "Evaluation of Free Space Optical (FSO) Link Under Weather Conditions in Abidjan," *Int. J. Phys.*, vol. 12, no. 6, pp. 247–259.

[10] Salih,M. G. M., Al-Dharrab,S. I., Alawsh,S. A., and Muqaibel,A. H. (2024). "Performance Analysis of Multi-Hop UAVs Using FSO Communications Under Humidity and Sandstorms Conditions," *IEEE Open J. Commun. Soc.*, vol. 5, pp. 6987–7001.

[11] Shen,B., Chen,J., Xu,G., Chen,Q., and Wang,J. (2023). "Performance Analysis of a Drone-Assisted FSO Communication System over Málaga Turbulence under AoA Fluctuations," *Drones*, vol. 7, no. 6, p. 374.

[12] Moon,H.J., Chae,C.B., Wong,K.K., and Alouini,M.S. (2025). "A Generalized Pointing Error Model for FSO Links With Fixed-Wing UAVs for 6G: Analysis and Trajectory Optimization," *IEEE Trans. Wirel. Commun.*, vol. 24, no. 7, pp. 5723–5737.

[13] INS, "Résultats globaux définitifs RGPH 2021," Institut National de la Statistique (INS). Accessed: May 05, 2026. [Online]. Available: https://rp2021.anstat.ci/.

[14] Kottek,M., Grieser,J., Beck,C., Rudolf,B., and Rubel,F. (2006). "World Map of the Köppen-Geiger climate classification updated," *Meteorol. Zeitschrift*, vol. 15, no. 3, pp. 259–263.

[15] Silué, S., Kouassi, A. A., Dago, D. N., Dajuma, A., Doumbia, M., Touré, D. E., Kéita, S. (2021). "Assessing seasonal climate variability impact on the malaria patient's cases in the north of Côte d'Ivoire," *Adv. Image Video Process.*, vol. 9, no. 6.

[16] Jérôme,A.N. (2022). "Kafoudal," *Rev. des Sci. Soc. l'université Peleforo Gon Coulibaly korhogo*, vol. 3–4, p. 316.

[17] Elamassie,M. and Uysal,M. (2023). "Free Space Optical Communication: An Enabling Backhaul Technology for 6G Non-Terrestrial Networks," *Photonics*, vol. 10, no. 11, p. 1210.

[18] Kim,I. I., and Korevaar,E. J., "Availability of free-space optics (FSO) and hybrid FSO/RF systems," E. J. Korevaar, Ed., Nov. 2001, p. 84.

[19] Kaushal, H. and Kaddoum,G. (2017). "Optical Communication in Space: Challenges and Mitigation Techniques," *IEEE Commun. Surv. Tutorials*, vol. 19, no. 1, pp. 57–96.

[20] Yao, C., Kacou, M., Koffi, E. S, Dao, A., Dutremble, C., Guilliod, M., Kamagaté, B., Perrin, J-L., Salles, C., Neppel, L., Paturel, J-E., Zahiri, E. P., Séguis, L. (2024). "Rainfall risk over the city of Abidjan (Côte d'Ivoire): first contribution of the joint analysis of daily rainfall from a historical record and a recent network of rain gauges," *Proc. IAHS*, vol. 385, pp. 259–265.

[21] Ghoname,S., Fayed,H. A., El Aziz,A. A., and Aly,M. H. (2017). "FSO System Performance Enhancement: Receiver Impact," *J. Adv. Res. Appl. Mech.*, vol. 37, no. 1, pp. 1–8.

[22] Elamassie,M. and Uysal,M. (2022). "Aerosol Attenuation Model for High Altitude UAV-Based FSO Links," in *2022 13th International Symposium on Communication Systems, Networks and Digital Signal Processing (CSNDSP)*, IEEE, Jul. 2022, pp. 71–75.

[23] Ajam,H., Najafi, M., Jamali,V., and Schober,R. (2020). "Ergodic Sum Rate Analysis of UAV-Based Relay Networks With Mixed RF-FSO Channels," *IEEE Open J. Commun. Soc.*, vol. 1, pp. 164–178.

[24] Chapala,V. K. and Zafaruddin,S. M. (2022). "Unified Performance Analysis of Reconfigurable Intelligent Surface Empowered Free-Space Optical Communications," *IEEE Trans. Commun.*, vol. 70, no. 4, pp. 2575–2592.

[25] Ai,D. H., Trung,H. D., and Tuan,D. T. (2020). "On the ASER performance of amplify-and-forward relaying MIMO/FSO systems using SC-QAM signals over log-normal and gamma-gamma atmospheric turbulence channels and pointing error impairments," *J. Inf. Telecommun.*, vol. 4, no. 3, pp. 267–281.

[26] Trung,H. (2021). "Performance of UAV-to-Ground FSO Communications with APD and Pointing Errors," *Appl. Syst. Innov.*, vol. 4, no. 3, p. 65.

[27] Ansari,I. S., Yilmaz,F., and Alouini,M.-S. (2016). "Performance Analysis of Free-Space Optical Links Over Málaga ($\mathcal{M}$) Turbulence Channels With Pointing Errors," *IEEE Trans. Wirel. Commun.*, vol. 15, no. 1, pp. 91–102, Jan. 2016.

[28] Alheadary,W. G., Park,K.H., and Alouini,M.S. (2017). "Performance analysis of multihop heterodyne free-space optical communication over general Malaga turbulence channels with pointing error," *Optik (Stuttg).*, vol. 151, pp. 34–47.

[29] ANAM, "Historique des prévisions météo à Korhogo." Accessed: May 10, 2026. [Online]. Available: https://www.historique-meteo.net/afrique/cote-d-ivoire/korhogo/2026/.

[30] Gnamien, S., Yoboué, V., Liousse, C., Ossohou, M., Keita, S., Bahino, J., Siélé, S., Diaby, L. (2021). “Particulate Pollution in Korhogo and Abidjan (Cote d’Ivoire) during the Dry Season,” *Aerosol Air Qual. Res.*, vol. 21, no. 1, p. 200201.

[31] Xu,M., Xu,G., Dong,Y., Wang,W., Zhang,Q., and Song,Z. (2023). “UAV-assisted FSO communication system with amplify-and-forward protocol under AOA fluctuations: A performance analysis,” *China Commun.*, vol. 20, no. 11, pp. 111–130.

[32] Ahmed,H. Y., Zeghid,M., Khan,A. N., and Abd El-Mottaleb, S. A. (2025). “Fuzzy Logic-Based Performance Enhancement of FSO Systems Under Adverse Weather Conditions,” *Photonics*, vol. 12, no. 5, p. 495.

[33] Bayraktar,M., Garces, S.L. M., Duncan,J. C. M., and Chatzinotas,S., “Rytov Variance of Adaptive Optics Applied Modified Von-Karman Spectrum,” in *2024 IEEE Wireless Communications and Networking Conference (WCNC)*, IEEE,pp. 1–5.

[34] Gao,W., Han,C., and Chen,Z. (2023). “Scintillation and Attenuation Modelling of Atmospheric Turbulence for Terahertz UAV Channels,” *arXiv Prepr. arXiv2305.08820*.

[35] Moon,H.J., Chae,C.B., Wong,K.K., and Alouini,M.S. (2025). “A Generalized Pointing Error Model for FSO Links With Fixed-Wing UAVs for 6G: Analysis and Trajectory Optimization,” *IEEE Trans. Wirel. Commun.*, vol. 24, no. 7, pp. 5723–5737.